NASA
Technical
Paper
2524

October 1985

Verification of Computer-Aided Designs of Traveling-Wave Tubes Utilizing Novel Dynamic Refocusers and Graphite Electrodes for the Multistage Depressed Collector

Peter Ramins,
Henry G. Kosmahl,
Dale A. Force,
Raymond W. Palmer,
and James A. Dayton, Jr.

NASA

NASA Technical Paper 2524

1985

Verification of Computer-Aided Designs of Traveling-Wave Tubes Utilizing Novel Dynamic Refocusers and Graphite Electrodes for the Multistage Depressed Collector

Peter Ramins,
Henry G. Kosmahl,
Dale A. Force,
Raymond W. Palmer,
and James A. Dayton, Jr.

Lewis Research Center
Cleveland, Ohio

National Aeronautics and Space Administration

Scientific and Technical Information Branch

Trade names or manufacturers' names are used in this report for identification only. This usage does not constitute an official endorsement, either expressed or implied, by the National Aeronautics and Space Administration.

Summary

Experimental verification is presented for a computational procedure to design and analyze a traveling wave tube (TWT) with a refocusing system and a multistage depressed collector (MDC). Two components not previously implemented in this type of computational procedure are described—namely, the dynamic analysis of the refocusing system, and a semi-quantitative analysis of the secondary electron trajectories in the MDC.

In addition, the MDC electrodes are fabricated from a particular form of isotropic graphite chosen for its low secondary electron yield, thermal expansion characteristics, machinability, and vacuum properties. The TWT has a minimum output of 200 W over the band from 8 to 18 GHz. The four-stage collector has an active diameter of 1.7 cm.

As in previous work of this kind, multidimensional computer programs are used to describe the interaction of the electron beam with the electric and magnetic fields of the TWT, refocuser, and MDC. The electron beam is modeled as a series of 32 disks of charge per RF cycle; the trajectories of the disks are computed from the RF input to their impacts on the electrodes of the MDC.

The electron beam in the refocuser is analyzed as a time-dependent, or dynamic, beam rather than as a steady-state, or continuous, beam. By treating the refocuser dynamically, the spent-beam energy distribution can be modified to account for the dissipation of axial space charge (debunching). With the steady-state analysis used formerly, only the effects of radial space charge can be considered, and the spent beam energy distribution is virtually unchanged in the refocuser.

The secondary electron analysis introduced here is semi-quantitative. Representative beams of secondary electrons are introduced into the MDC analysis, and their trajectories are computed.

The MDC was tested in CW mode for more than 1000 hr with negligible degradation in TWT and MDC performance. The MDC was designed and tested as a four-stage collector, but was also analyzed and operated as a three-stage collector.

The maturity of the computer-aided design procedure is indicated by the very good efficiency obtained; experimental optimization was limited to adjustments of the electrode voltages. Computed MDC efficiency and TWT performance are in good agreement with measured quantities.

Introduction

In earlier reports (refs. 1 to 3), a computational procedure for the design of TWT-refocuser-MDC systems was presented. The present paper extends this work to—

(1) short "dynamic refocusing" systems (simultaneous beam debunching and reconditioning);

(2) a semi-quantitative treatment of secondary emission losses in MDC's;

(3) an improved modeling of the periodic permanent magnet (PPM) stack characteristics; and

(4) collectors of very small size.

Furthermore, the performance of a new MDC electrode material, POCO Graphite, Inc., DFP-2, is described.

The work was conducted at the NASA Lewis Research Center under a joint NASA-USAF program to improve the performance of TWT's for use in communication and electronic countermeasure systems, and to reduce the risk, time, and cost of tube acquisition. A key element of this program has been the development of computer-aided design techniques for the TWT-refocuser-MDC system.

In references 1 to 3, the computer models were described in detail, and comparisons were made for a number of TWT-refocuser-MDC systems with separate spent beam debunching sections and relatively long, solenoid refocusers. In general, very good agreement was found between computed and measured TWT-MDC performance.

In a continuation of this program, the work has been extended to the design of short, permanent-magnet, "dynamic refocusing" systems situated next to the RF output of the TWT and to the semi-quantitative treatment of secondary electron emission losses in MDC's. In the former, the large-signal TWT computer program, rather than the steady-state, Herrmannsfeldt Electron Trajectory Program (ref. 4), is used to model charge trajectories through the refocusing section. In the latter, representative charges are injected into the MDC from the locations where primary charges from the spent beam impinge on the collector electrodes.

The computational design technique was used to design a short, permanent-magnet refocuser and small three-and four-stage depressed collectors for an existing 8- to 18-GHz, TWT (Varian Assoc., Inc., Model VTM-6294). The refocuser and four-stage collector designs were fabricated, and an experimental program was conducted to evaluate the TWT-MDC performance under a variety of operating conditions.

In the following, the computer models, the analytical and experimental procedures, and the tube characteristics are briefly described; the results of the TWT, refocuser, and MDC analyses are discussed; and comparisons of analytical and experimental results are presented. The performance of the TWT/MDC across its operating band is discussed, as is the performance of the new isotropic graphite electrode material.

Symbols

B_z axial magnetic field, T

I_B intercepted-beam current, A

I_G total body current, including backstreaming from collector, A

I_0 beam current, A

P_{body} body power, sum of RF circuit losses and intercepted-beam power in forward direction, W

P_{coll} collector power, $V_0I_0-P_{RF}-P_{body}$, W

P_{rec} recovered power, $\sum_{n=1}^{4} |V_0 - V_{en}|I_{en}$, W

P_{RF} total RF output power, W

P' prime power, $V_0I_G+\sum_{n=1}^{4} V_{en}I_{en}$, W

V_0 cathode potential with respect to ground, V

η_{coll} collector efficiency, P_{rec}/P_{coll}, percent

η_e TWT circuit efficiency, $P_{RF}/(P_{RF}+$circuit losses), percent

η_{ov} TWT overall efficiency, $P_{RF}/$(dc input power), percent

η_{RF} RF efficiency of TWT, P_{RF}/V_0I_0, percent

Analytical Models and Computer Programs

Overall System

Flow diagrams illustrating the distributions of power and electron current are shown in figure 1 for the TWT-refocuser-MDC system. For the purpose of analysis, the system was divided into three parts: (1) the TWT between the RF input and output; (2) the "dynamic refocusing" region; and (3) the MDC. The first two parts of the calculation were performed using the NASA Lewis Research Center's large-signal, multidimensional, helical TWT program. In this program, the electron beam is divided into 32 disks (or alternately 96 rings) of charge per RF cycle, and trajectories of the disks are tracked through the tube and the dynamic refocusing system. In part (3) of the calculation, the trajectories of the 32 representative charges were computed using the Herrmannsfeldt Electron Trajectory Program (ref. 4).

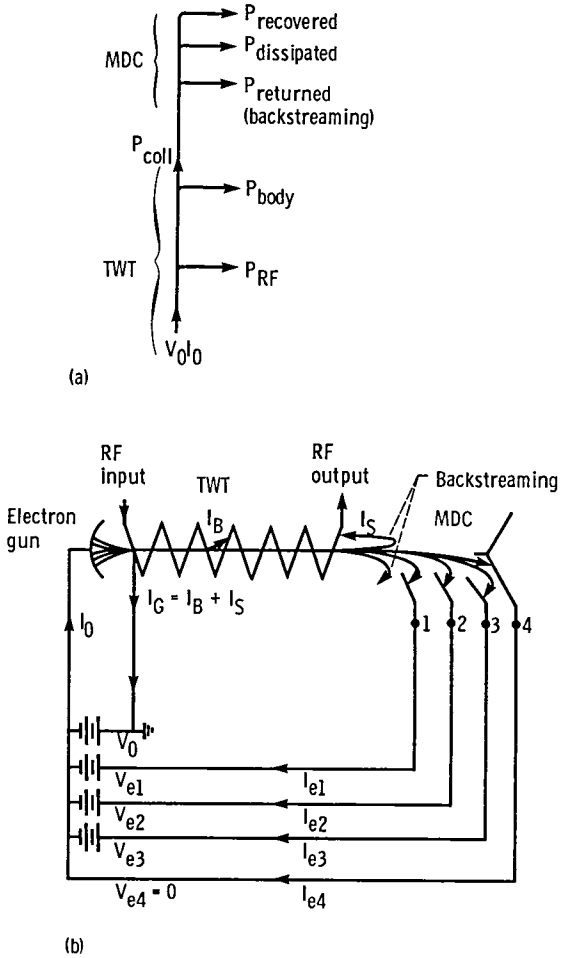

(a) Power flow.
(b) Electron flow.

Figure 1.—Flow diagrams for TWT with four-stage, depressed collector.

Traveling Wave Tube

In the TWT, disk trajectories in the presence of RF circuit forces, space charge forces, and magnetic focusing fields are computed from the RF input of the TWT to the RF output. At the RF output, the computer program lists the following:

(1) RF output power

(2) RF circuit losses

(3) Sever and attenuator losses
(4) Intercepted current and power
(5) Radial coordinates of the disk edges
(6) Three components of velocity ($\dot{r}$, $\dot{\varphi}$, $\dot{z}$) of each disk
(7) Relative phase of each disk

The trajectory program does not include effects of thermal velocities on the radial and azimuthal motion. According to Herrmann's optical theory of thermal electrons, these effects should be relatively small for a tube such as this with a perveance of 0.255×10^{-6}.

At the RF output, the electron beam is tightly bunched, causing strong space charge forces to exist between disks.

The cosine approximation used formerly to describe the PPM magnetic field has been replaced in the present work by a more accurate simulation of the magnetic field of the PPM stack. The field is obtained by computing the first three odd terms of the equation

$$B_z(z,r) = \sum_{n=1}^{\infty} \frac{4B_0 \sin\left(\frac{n\pi g}{L}\right)}{I_0\left(\frac{nd}{L}\right)} \times I_0\left(2n\pi \frac{r}{L}\right) \cos\left(2n\pi \frac{z}{L}\right)$$

where

B_0 field in the gap between the polepieces

g length of the gap

d polepiece diameter

I_0 modified Bessel function of the first kind of order zero

The radial field is computed using the fact that the divergence of the magnetic field is zero.

Dynamic Refocusing System

The description of the spent beam at the RF coupler of the TWT provides the input data for the refocusing system calculations. The refocusing system is situated next to the RF output coupler, and simultaneous beam debunching and reconditioning is accomplished. The beam characteristics at the end of the refocusing section define the input conditions to the MDC.

A recent modification in the method of utilization of the TWT program permits the stable computation of the electron beam flow in a region where the tunnel diameter changes discontinuously. This permits the analysis of a wide variety of possible refocuser configurations. The effect on the spent beam of debunching and reconditioning in the refocuser now can be treated simultaneously.

Multistage Depressed Collector

The computation of the trajectories in the MDC treats the 32 disks as continuous rays of current; that is to say, complete debunching is assumed. Each current ray is located at the centroid of charge of its corresponding disk and has the vector velocity of the disk centroid. The trajectory calculation is continued until the current rays impact the MDC electrodes. The effect of secondary electron emission from electrode surfaces is analyzed by injecting one or more representative subcharges at the points of impact of the primary current-rays and tracking their trajectories to their final termination within the MDC or TWT. The effects of further secondary electron emission due to these secondaries are neglected. Based on the final location of the primary and secondary charges, a calculation is made of the collected current, recovered power, and dissipated power at each of the collector electrodes and, if backstreaming occurs, at the TWT itself. These results, when coupled with the outputs of the TWT computer program, provide a detailed picture of the current and power flow within the TWT-MDC system.

Characteristics of Traveling-Wave Tube and Multistage Depressed Collector

A modified version of Varian TWT model VTM-6294 was used in this program. The VTM-6294 has a helix slow wave circuit and PPM focusing. Two permanent magnets past the RF output coupler, in a continuation of the PPM stack, constituted the refocusing system of 1.25 magnetic periods. The general tube operating characteristics were as follows:

Frequency, GHz	8 to 18
Beam voltage, kV	9.2 to 9.8
Beam current, A	0.23 to 0.255
Minimum saturated output power, W	200
Duty cycle, percent	100 (CW)

A NASA Lewis designed and fabricated MDC, shown in figure 2, utilizing four separate brazed-graphite electrodes was used in these tests. The MDC was designed to be conduction cooled to the existing TWT baseplate. The MDC contained considerably more graphite than actually required, because it was designed to utilize existing alumina insulating rings (fig. 2). The MDC was delivered to Varian for integration with the TWT, bakeout, and RF focusing/processing.

Analytical and Experimental Procedure

The computational design procedure was used to design a refocusing system and three- and four-stage

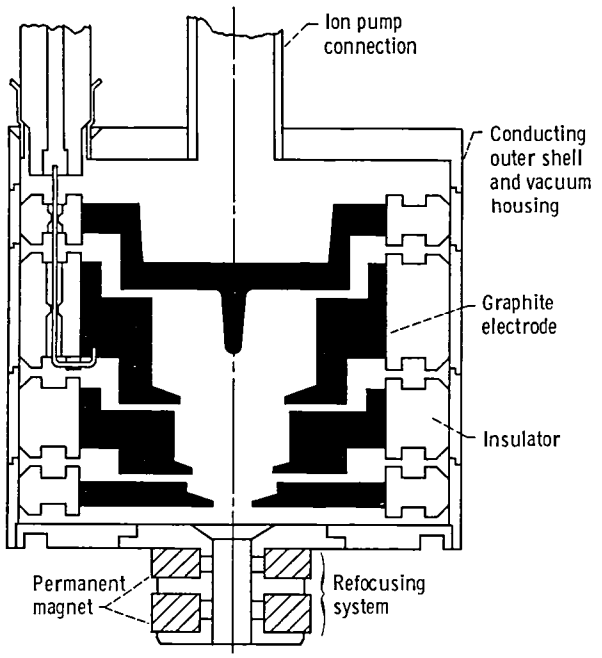

Figure 2.—Cross section of four-stage, brazed-graphite, depressed collector and permanent magnet refocusing system.

depressed collectors for the TWT, with small size, simplicity, and ease of fabrication in mind. The TWT computer analysis was done at saturation at the midband frequency of 13 GHz (where the greatest electronic efficiency was expected to occur) using the 32-disk model and the recently implemented improved formulation in the modeling of the PPM stack described previously.

Since the TWT already has two, full-strength, permanent magnets past the RF output coupler of the TWT, the plan was to attempt to design an efficient MDC for the beam after it had transversed this continuation of the PPM stack for 1.25 magnetic periods, a[illegible] resort to separate refocusing optimization only if high collector efficiencies could not be obtained. This optimization was not necessary.

The collectors were designed before the semi-quantitative technique for evaluating secondary electron emission losses was implemented; had this been available, the collector designs would have been modified slightly.

A TWT, equipped with the four-stage collector was fabricated and experimentally evaluated at a number of distinct TWT-MDC operating conditions, including—

(1) analytical design collector voltages at 13 GHz;
(2) experimentally optimized collector voltages at 13 GHz;
(3) intermediate collector voltages at 13 GHz; and
(4) experimentally optimized MDC voltages for operation of the TWT across its full bandwidth.

The MDC analyses were then performed for operating conditions (2) to (4).

In the case of the three-stage collector, it was found analytically that virtually identical MDC performance could be obtained with the three-stage simulation using the four-electrode collector. In this simulation, electrodes 1 and 2 were electrically connected (the number of collector stages is defined as the number of distinct voltages, other than ground, required to operate the MDC.). The actual and simulated three-stage designs and performances will be shown later. Because of the similar performance, the three-stage MDC was not constructed, and the TWT equipped with the four-electrode collector hooked up in a three-stage configuration was evaluated at operating conditions (1) to (3) described previously. The TWT-MDC performance was then analyzed at these collector operating conditions. The following sections give the results of the TWT, refocusing system, and MDC analysis and present a comparison of the analytical and experimental TWT and three- and four-stage collector performance for the operating conditions described previously.

However, because the TWT was not operated first with an undepressed collector (which produces only negligible backstreaming power) and the TWT and the MDC electrodes were conduction cooled to a single baseplate, it was not possible to present the detailed picture of power flow in the experimental TWT and MDC given in references 1 to 3. Furthermore, the computation of collector efficiency required the making of certain assumptions (discussed later).

Results of Traveling Wave Tube Analysis and Comparison with Measurements

The computed and measured RF performance is shown in table I. Since the tube operating parameters for the analytical design case and the experimental TWT (called TWT 204 hereinafter) differ somewhat, the results in this and in subsequent sections of this report are shown as percentages of I_0, V_0, and I_0V_0,. The results are in relatively good agreement. The highest RF efficiency of TWT 204, 13.5 percent, occurred at 15.0 GHz.

The computed spent-beam energy distributions before and after debunching, for operation of the TWT at saturation, are shown in figure 3. As observed previously in references 1 to 3, the debunching action substantially alters the spent-beam energy distribution.

Refocusing System Analysis Results

The very simple focusing system consisting of two full-strength magnets past the RF output coupler, in a continuation of the PPM stack, was found to be

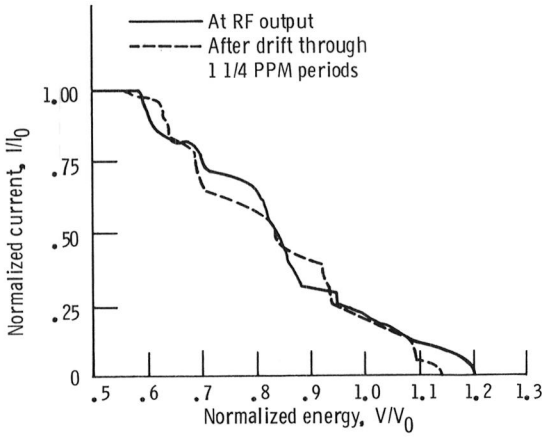

Figure 3.—Computed spent-beam energy distributions before and after debunching for TWT operation at saturation. Electronic efficiency, η_e, 0.162; perveance, 0.28×10^{-6} $A/V^{3/2}$.

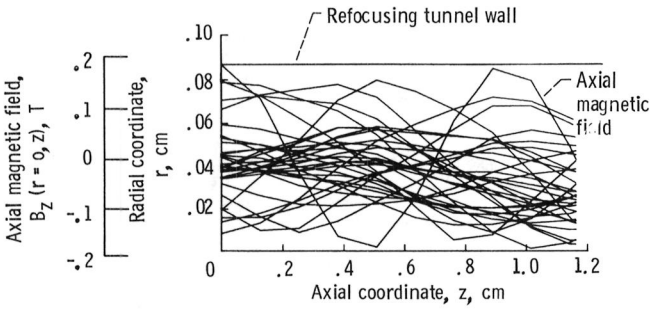

Figure 4.—Charge trajectories and refocusing field profile in refocusing section for TWT operation at saturation.

acceptable. The beam debunching in the refocuser has already been discussed. The charge trajectories through the refocusing region are shown in figure 4. The disk edge angles and radii at the input to and the output of the refocuser are shown in tables II and III. The number of negative angles has been increased, and the average beam radius reduced (compression rather than controlled beam expansion). On the surface, this does not appear to be a good refocusing system. However, as will be discussed in the next section, it was possible to design highly efficient collectors for this beam. Consequently, this refocusing system was selected for its simplicity and ease of fabrication (the TWT already had two magnets past the RF output).

Multistage Depressed Collector Analysis Results And Comparison With Measurements

Traveling Wave Tube and Four-Stage Collector

The four-stage, axisymmetric, MDC geometry, the applied potentials, the equipotential lines, and the charge

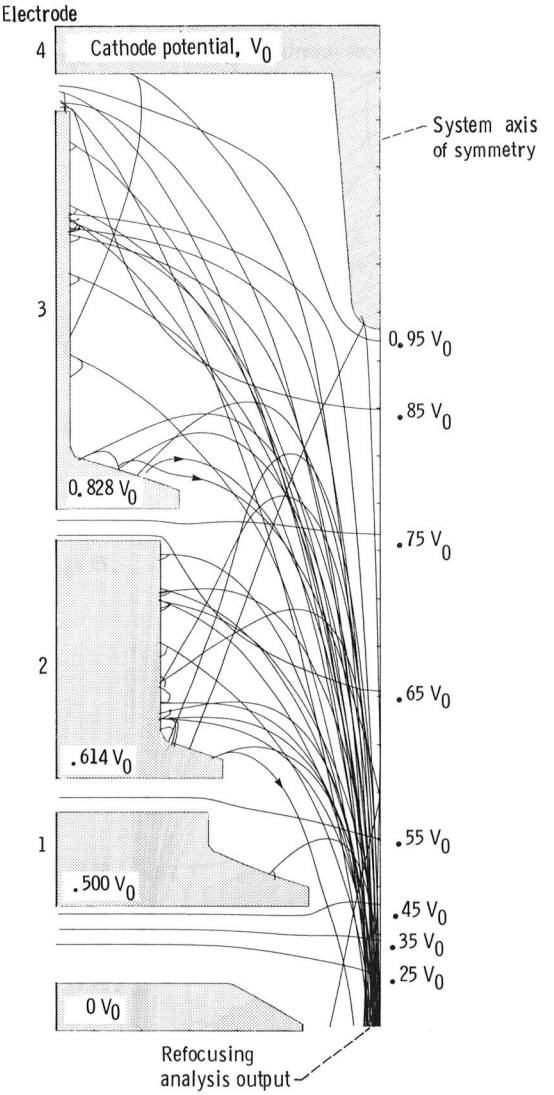

Figure 5.—Charge trajectories in four-stage, 1.7-centimeter-diameter, depressed collector operating at analytically determined voltages. TWT operating at saturation.

trajectories are shown in figures 5 to 8 for the cases of analytically determined voltages, intermediate voltages, experimentally optimized voltages, and the compromise, full-bandwidth operation voltages, respectively. The analytical and experimental TWT-MDC performances are compared in detail in tables IV to VII. Table VII also shows the measured TWT-MDC performance at the operating frequency (15 GHz) yielding the highest RF efficiency. The results, in terms of the TWT overall and the collector efficiencies, are summarized in table VIII(a). (The three-stage collector results, shown in table VIII(b), will be discussed in the following section of this report.) The computed collector current distributions shown in tables IV to VII include the effects of representative secondary electron emission from the electrode surfaces. These are for the case of slow (10 eV) electrons injected back along the angle of incidence (the

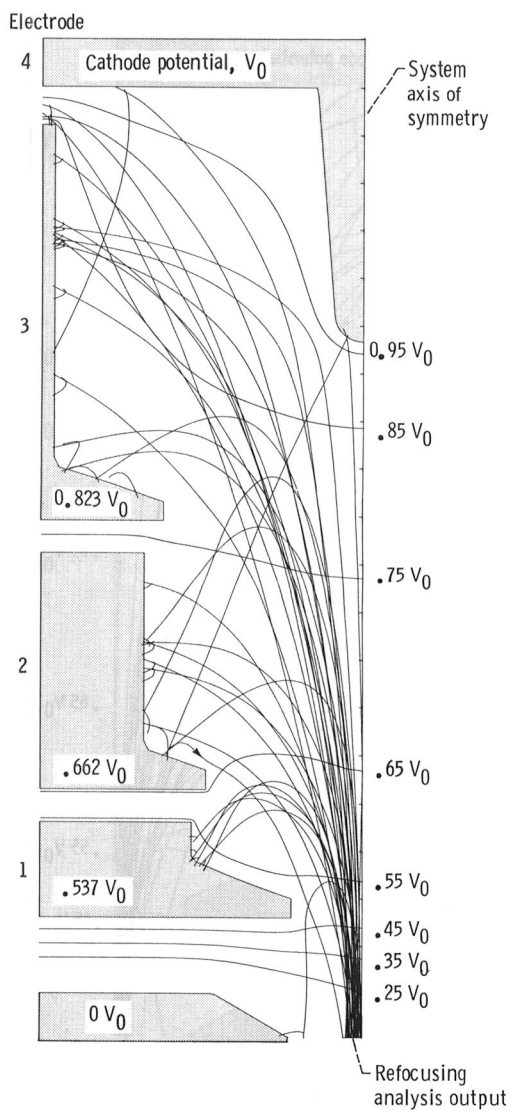

Figure 6.—Charge trajectories in four-stage, 1.7-centimeter-diameter, depressed collector operating at intermediate voltages. TWT operating at saturation.

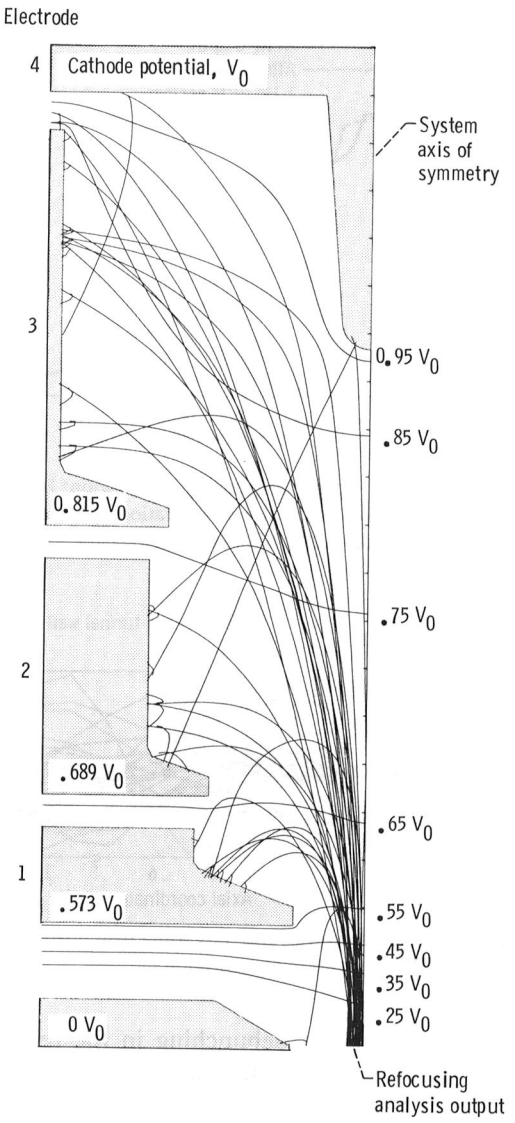

Figure 7.—Charge trajectories in four-stage, 1.7-centimeter-diameter, depressed collector operating at experimentally optimized voltages. TWT operating at saturation.

most probable angle in some cases) in the amount $I_i(0.4+0.2\theta^2)$, where θ is the angle of incidence in radians, and I_i is the incident current. Secondary electrons have, in fact, angular and energy distributions which depend on the angle of incidence, the energy of the incident electrons, and the electrode surface material and characteristics. A better simulation (other energies and angles of injection) is readily possible; however, detailed measurements of secondary electron emission characteristics (the angular and energy distributions) of modern MDC electrode materials (e.g., POCO DFP-2 graphite) are not generally available. Furthermore, more complex simulations involve additional computer time and may not be cost-effective.

The trajectories of this one class of slow secondary electrons are shown in figures 4 to 7. The resulting degradations in the overall and the collector efficiencies are summarized in table IX.

Figures 5 and 6 show that, in some cases, slow secondary electrons generated over certain regions of even the "top" surfaces of the collector electrodes can backstream to the TWT itself. Clearly, such situations should be avoided by modified collector design or electrode operating potentials. Figures 5 and 7 and tables IV and VI clearly show the effect of secondary emission on MDC efficiency. The original design presumed the electrons incident on the upper surfaces of the MDC electrodes produced secondaries that were trapped by the local electric fields and recollected on the same electrode. Subsequently, the computation of secondary emission trajectories was added to the analysis. On electrode 3 in figure 5 it can be seen that two of the secondary

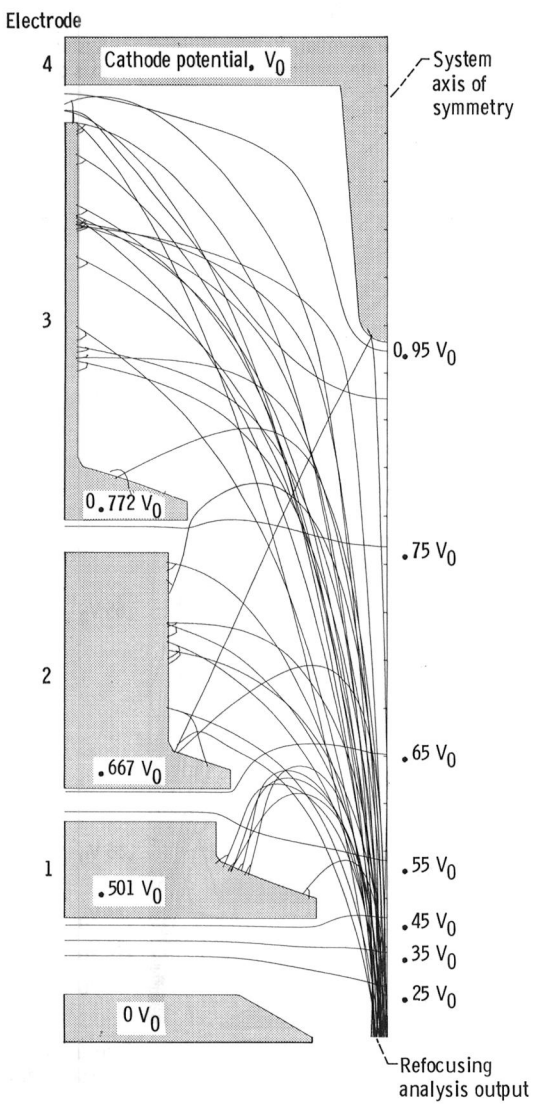

Figure 8.—Charge trajectories in four-stage, 1.7-centimeter-diameter, depressed collector operating at voltages selected for 8- to 15.5-GHz operation at saturation.

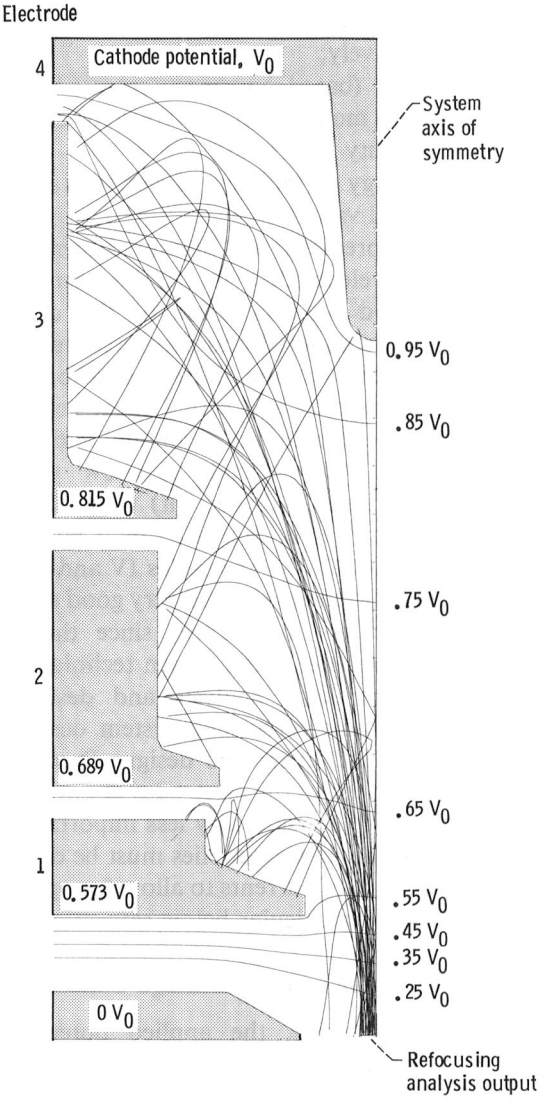

Figure 9.—Charge trajectories of incident and of elastically reflected primaries in four-stage, depressed collector. TWT operating at saturation.

trajectories are not collected but stream back to the tube body. In experimentally optimizing the MDC, the third stage was less depressed, with the result that the analysis indicates all the secondaries are recollected. The current to the third stage is accordingly increased; the recovered power increases, even though the stage is less depressed.

In experimentally optimizing the collector, the depression of stages 1 and 2 was increased. This had the effect of rejecting the lowest energy current ray in the spent beam (which experimental results indicate had, in fact, greater energy), and eliminating backstreaming secondary emission from electrode 2. Analytically, the total recovered power on these two stages was unchanged, while the kinetic dissipation decreased; experimentally, the total recovered power increased.

The losses due to elastically and inelastically scattered primary (high energy) electrons may be at least as important as those due to true secondaries; however, only very limited quantitative data have been found on this component of secondary electron emission in modern MDC's.

The trajectories of elastically reflected primary electrons injected back along the angle of incidence are shown in figure 9. When other possible angles of injection are considered, it is clear they could end up almost anywhere in the collector or TWT. Because of the lack of data on reflected primaries from POCO DFP-2 graphite, no attempt was made to quantify these losses.

As discussed previously, since the TWT was not first operated with an undepressed collector, certain assumptions had to be made in order to compute collector efficiencies. The assumptions used were—

(1) circuit efficiencies of 0.75 and 0.73 at 13 and 15 GHz, respectively;
(2) $I_B = 4.5$ mA (based on measurements for several TWT's of this model with zero collector depression,[1] at very low duty cycle); and
(3) average energy of intercepted electrons of 0.98 V_0 (the computed value).

Comparing the predicted and measured currents to the various collector electrodes, it can be seen that the agreement is good only in some of the cases. The differences in the computed and measured currents can largely be explained by subtle differences of only 5 to 10 percent in the computed and actual spent-beam energy distributions. For example, the computed and measured values of current to electrode 3 show very good agreement (42.6 versus 44.2 percent) when the applied voltage to the electrode is decreased by 7 percent (i.e., from 0.828 V_0 to 0.772 V_0—see tables IV and VII).

The collector efficiencies showed very good agreement. This is of particular importance, since the primary purpose of the computer-aided design techniques, apart from TWT performance analysis and design, is to produce an acceptable refocusing system design and a highly efficient MDC geometric design. Predicting the distribution of current to the electrodes at one particular operating point is of considerably less importance, since the collector and the power supplies must be designed to tolerate a wide range of currents to allow for operation at other conditions, in particular below saturation.

Traveling Wave Tube and Three-Stage Collector

The MDC geometries, the applied potentials, the equipotential lines, and the charge trajectories for the three-stage collector and the three-stage simulation using the four-electrode collector are shown in figures 10 and 11, respectively, for the case of analytically determined (optimized) voltages. The collector current distributions and the overall and MDC efficiencies are compared in table X. It is apparent that the computed performance of these designs is virtually identical. Consequently, a separate TWT equipped with the three-stage collector was not fabricated; instead, TWT 204, with the four-electrode collector operated as a simulated three-stage, was used to evaluate the TWT and three-stage collector performance.

The applied potentials, the equipotential lines, and the charge trajectories are shown in figures 11 to 13 for the cases of analytically determined voltages, intermediate voltages, and experimentally optimized voltages, respectively. Analytical and experimental TWT-MDC performances are compared in detail in tables XI to XIII. The results, in terms of the TWT overall and collector

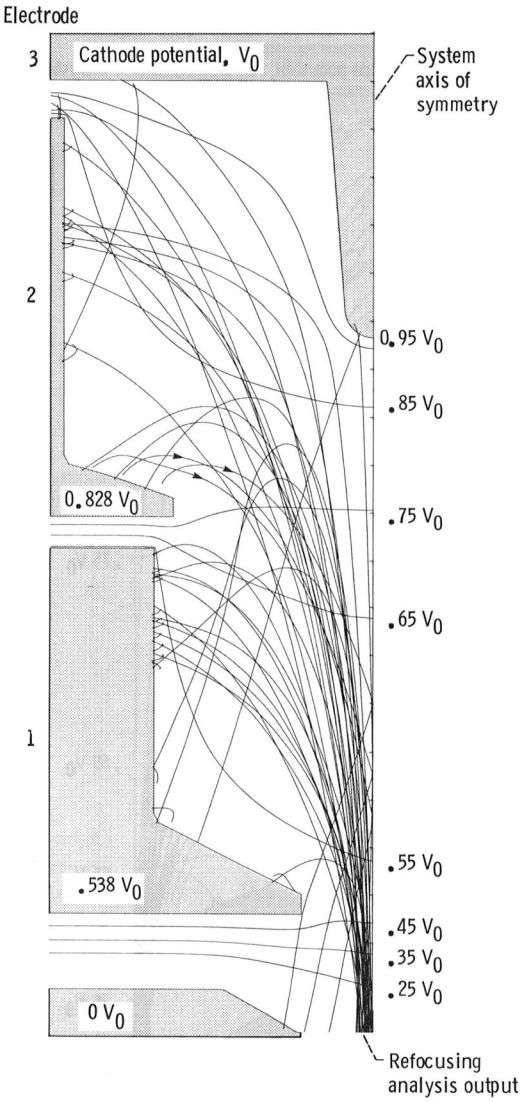

Figure 10.—Charge trajectories in three-stage, 1.7-centimeter-diameter, depressed collector operating at analytically determined voltages. TWT operating at saturation.

efficiencies, are summarized in table VIII(b). The degradations in the overall and the collector efficiencies due to the computed secondary electron emission losses are summarized in table XIV. Assumptions identical to those used to compute the four-stage collector efficiencies also were used to compute the three-stage collector efficiencies and the secondary emission losses in the three-stage collector.

A comparison of computed and measured results shows trends and leads to conclusions similar to those reached previously for the four-stage collector.

The combination of computer-aided MDC geometric design and experimental optimization of its operating voltages produced a very good first design. Furthermore, the experimentally optimized collector efficiency is surprisingly high in view of the compressed, disordered beam at the output of the refocuser. However, when the

[1] Data supplied by Varian Associates, Inc.

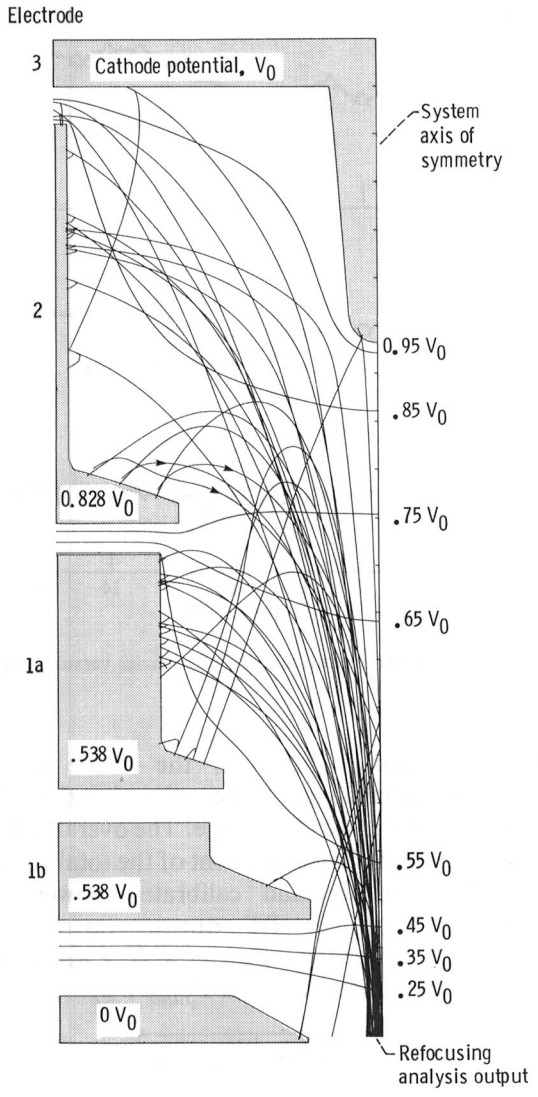

Figure 11.—Charge trajectories in simulated three-stage, 1.7-centimeter-diameter, depressed collector operating at analytically determined voltages. TWT operating at saturation.

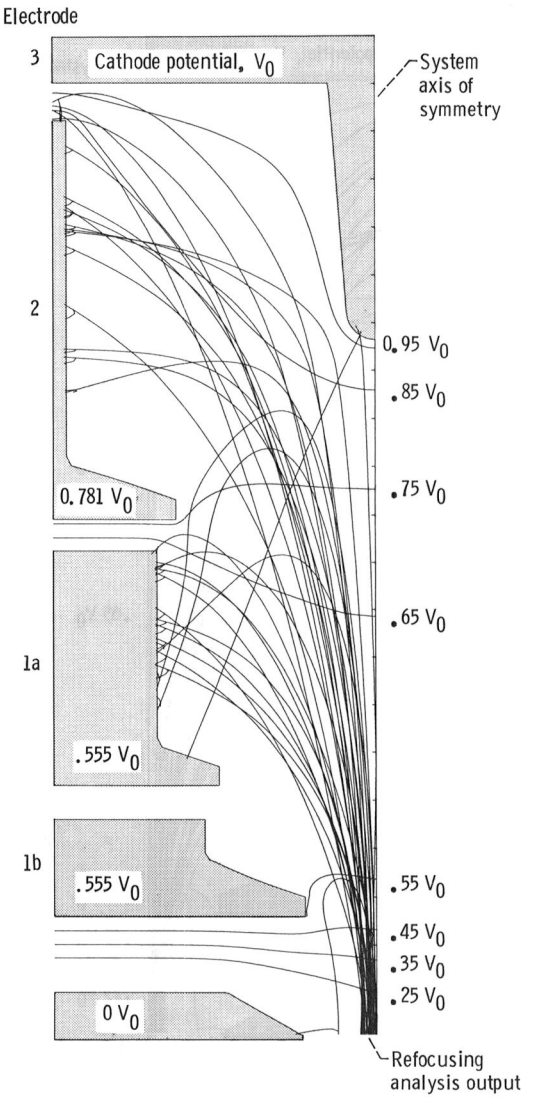

Figure 12.—Charge trajectories in three-stage, 1.7-centimeter-diameter, depressed collector operating at intermediate collector voltages. TWT operating at saturation.

beam size at the MDC input is much smaller than the collector size, positive and negative angles become indistinguishable to the collector.

At the outset of this program, it was envisioned that the refocusing system profile would be optimized by individually trimming the strength of the two refocusing-system magnets, within the range of ± 10 percent, and by shunting the magnets to optimize the TWT overall efficiency. However, the "packaged" TWT/MDC delivered by Varian did not provide ready access to the refocusing system. Because of the favorable results obtained with the nominal refocuser, and because of the risk involved in the removal and reinstallation of the coaxial-to-waveguide adapter (a delicate procedure), such optimization was not performed. In general, it should be performed at the manufacturer's facility during low-duty-cycle, pulsed operation, while real-time readouts of the power recovered in the collector and the body current are monitored.

Traveling Wave Tube and Multistage Depressed Collector Performance Across Operating Bandwidth

The TWT and four-stage collector performance was evaluated across its useful operating band. This turned out to be 8 to 15.5 GHz, limited in the upper end of the band by a poor output match for a range of frequencies above 16 GHz. The MDC voltages used (see table VII) had to be reduced considerably from their optimum values at midband (see table VI) because of a large increase in body current (backstreaming from the

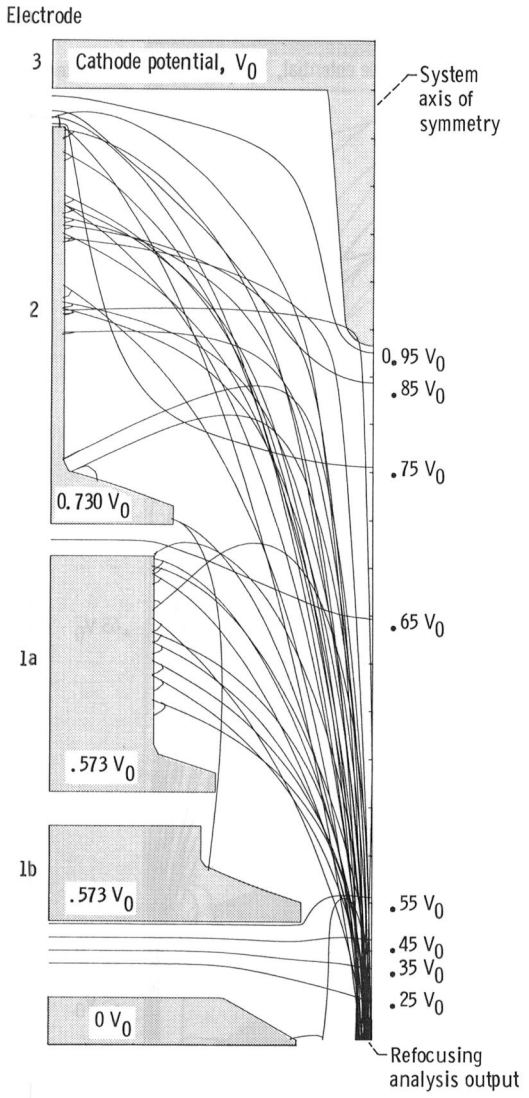

Figure 13.—Charge trajectories in three-stage, 1.7-centimeter-diameter, depressed collector operating at experimentally optimized voltages. TWT operating at saturation.

collector) for operation in the range of frequencies of 8.5 to 10.5 GHz, where a significant second harmonic content is present in the RF output power. In these tests, filtered input power was used at and below 12 GHz, and saturation was set with use of a power meter which measured filtered RF output power at the fundamental frequency. The results are shown in figure 14 and summarized in table XV.

In computing the collector efficiencies, a linear variation in TWT circuit efficiency from 0.8 at 8 GHz to 0.725 at 15.5 GHz and a constant intercepted beam power of 1.9 percent of I_0V_0 were assumed. Measurements with other tube types (e.g., ref. 5) have indicated that beam interception is higher over the lower parts of the operating band where a significant amount of harmonic power is produced and total TWT body power (sum of circuit losses and beam interception losses) is

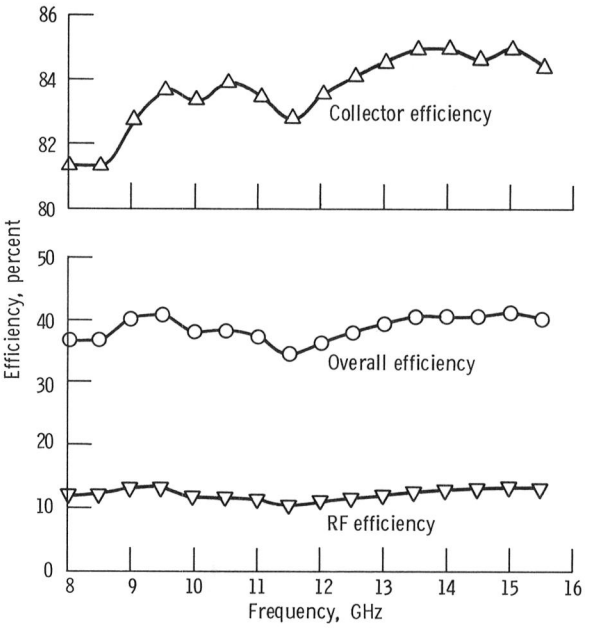

Figure 14.—Collector, overall, and RF efficiencies versus frequency at saturation.

relatively constant. Therefore, the above procedure probably results in slightly underestimating the collector efficiency in the 8 to 12 GHz range. The overall efficiency is based on a thermal measurement of the total RF output power. Power meter and calibrated power splitter measurements of the RF output power at the fundamental frequency, P_{fund}, and P_{RF} gave the following approximate ratios of P_{fund}/P_{RF}:

Frequency, GHz	P_{fund}/P_{RF}
8.0	0.84
8.5	.87
9.0	.86
9.5	.85
10.0	.86
10.5	.87
11.0	.86
11.5	.89
12.0	.87

Overall efficiency, based on P_{fund}, can be computed by using these values.

Performance of POCO DFP-2 Graphite as a Collector Electrode Material

The TWT and MDC were assembled, baked out, and dc-RF processed at Varian. The bakeout was performed in two stages (separated by a cathode activation procedure) for a total of 30 hr at 550 °C. Approximately

35 hr of pulsed dc aging (no RF) and over 30 hr gradual, CW, RF aging were required before saturated CW data could be obtained across the operating band. A 2-l/s ion pump at the collector (see fig. 2) was used throughout these tests.

The bakeout performance of the TWT/MDC was indistinguishable from the production TWT with its copper collector; however, the TWT/MDC was described as somewhat "gassy" at several early stages in the testing program at Varian. The above information was extracted from the tube log supplied by Varian. In all, ~130 hr of pulsed and CW aging and testing were accumulated at Varian.

During initial testing at Lewis, the 2-l/s ion pump was used continually. Pump currents, which ranged from 0.02 to 0.025 μA initially, dropped to virtually zero (<5 to 10 nA, the minimum detectable on the pump current readout) within about 100 hr of operation.

An extended test was started with the TWT operating at saturation at 15 GHz. After about 400 hr of CW operation, the ion pump was turned off entirely. In retrospect, this could probably have been done at the start of the long-term test. The testing was continued until over 1000 hr of CW operation had been accumulated. A daily check was made for a possible pressure buildup by turning the pump back on for a few seconds; no measurable pump current was ever detected.

During the first several hundred hours of operation, the body current rose (from 3 percent of I_0 to 5 percent) and the recovered power dropped about 20 W, the largest changes occurring early in the extended test program. The RF output power remained constant within 1 percent, but the saturated gain increased slightly. The overall efficiency decreased by 1 to 1.5 percentage points. It could not be definitely established whether the changes in body current and recovered power were due to changes in the TWT itself (larger beam due to improved outgassing of the TWT components), to small dimensional changes in the TWT or MDC, or to changes in the secondary electron emission characteristics of the graphite electrodes.

It should be noted that the MDC contained considerably more graphite material than actually required, since the collector (in its outer dimensions) was designed to fit the existing TWT baseplate and to use available alumina insulators from another collector design. It is estimated that the "packaged" outer diameter of this collector could be reduced to 3.4 cm (from 4.6 cm) and the volume of graphite between an outer diameter of 2 cm and an inner diameter of 3 cm eliminated, thereby considerably improving its "outgassing" performance.

Concluding Remarks

The computer-aided design techniques described here produced a very efficient multistage depressed collector (MDC) that needed only adjustments of electrode voltages to achieve high efficiency. The inclusion of semi-quantitative, secondary-electron analysis provides greater accuracy in the determination of the loss of efficiency due to this effect and illustrates how it can be minimized. More elaborate models of secondary emission can certainly be implemented if warranted by the availability of secondary yield data and computational costs. The dynamic spent-beam analysis permits the designer to take into account the changes in the spent-beam energy distribution resulting from debunching, enabling the design of short refocusers situated next to the RF output coupler of the traveling wave tube (TWT) and more accurate MDC modeling. In general, very good agreement was obtained between computed and measured TWT performance and MDC efficiency.

Operation of the experimental TWT across its octave bandwidth indicated that the tube produced considerably different spent beams in the mid- to upper-band parts (highest electronic efficiency) and near the low-band edge, where a significant amount of harmonic power was generated.

An effective compromise in MDC operating conditions (voltages) was found for saturated TWT operation. However, efficiency in the linear range would have been compromised because the collector voltages had to be reduced. Consequently, it would be useful, for wide-band operation, to perform the analysis at two or more frequencies, including a frequency near the low-band edge (with fundamental and harmonic power) and at the highest electronic efficiency.

The new type of graphite MDC electrode material, POCO DFP-2, performed well. However, considerably more experience with it is required before definitive conclusions on its suitability for electronic countermeasure systems and space TWT's can be made.

Lewis Research Center
National Aeronautics and Space Administration
Cleveland, Ohio, July 10, 1985

References

1. Dayton, James A., Jr., et al.: Analytical Prediction with Multidimensional Computer Programs and Experimental Verification of the Performance, at a Variety of Operating Conditions, of Two Traveling Wave Tubes with Depressed Collectors. NASA TP-1449, 1979.
2. Dayton, James A., Jr.; et al.: Analytical Prediction and Experimental Verification of Performance, at Various Operating Conditions, of a Dual-Mode Traveling Wave Tube with Multistage Depressed Collectors. NASA TP-1831, 1981.
3. Dayton, James A., Jr.; Kosmahl, Henry G.; and Ramins, Peter: Experimental Verification of the Multistage Depressed Collector Design Procedure for a High Perveance, Helix-Type, Traveling-Wave Tube. NASA TP-2162, 1983.
4. Herrmannsfeldt, W.B.: Electron Trajectory Program. SLAC-166, Stanford Linear Accelerator Center, Sept. 1973.
5. Ramins, Peter; and Fox, Thomas A.: Multistage Depressed Collector with Efficiency of 90 to 94 Percent for Operation of a Dual-Mode Traveling-Wave Tube in the Linear Region, NASA TP-1670, 1980.

TABLE I.—COMPUTED VERSUS MEASURED OPERATING PARAMETERS AND CW PERFORMANCE OF TWT ANALYTICAL DESIGN AND EXPERIMENTAL TWT 204

Parameter	Analytical design value	Experimental value for TWT 204
Operating parameters		
Cathode voltage, kV	9.30	9.60
Cathode current, mA	255	240
TWT performance at 13 GHz (midband)		
RF efficiency, percent	13.5	12.3
Electronic efficiency, percent	16.2	16.4
Circuit efficiency, percent	83.6	[a]75
Intercepted current, percent	4.2	1.9

[a]Estimated value based on measurements of other TWT types.

TABLE II.—INPUT AND OUTPUT ANGLES OF DISK EDGE OF REFOCUSING SYSTEM FOR SATURATED OPERATION

Trajectory	Input angle, deg	Output angle, deg
1	−4.3	−1.1
2	1.5	−1.3
3	.12	3.9
4	.75	.17
5	5.2	0.48
6	2.8	.38
7	2.1	−1.8
8	2.7	−4.0
9	1.7	0.25
10	1.6	−1.0
11	−2.2	3.9
12	7.1	−7.4
13	2.4	−3.2
14	2.3	.63
15	−.37	1.7
16	1.7	4.4
17	1.4	−1.5
18	.27	−2.0
19	−2.4	1.4
20	−5.1	−3.3
21	−1.2	7.7
22	−.16	3.1
23	−1.2	2.8
24	5.0	−2.3
25	−0.46	−3.3
26	−2.3	2.0
27	1.2	7.5
28	3.1	−4.5
29	4.1	−0.36
30	2.5	1.6
31	1.0	3.3
32	−.77	−.39

TABLE III.—INPUT AND OUTPUT RADII OF DISK EDGE OF REFOCUSING SYSTEM FOR SATURATED OPERATION

Trajectory	Input radius, mm	Output radius, mm
1	0.27	0.54
2	.41	.24
3	.40	.27
4	.60	.10
5	0.66	0.03
6	.71	.05
7	.46	.19
8	.35	.26
9	0.34	0.28
10	.14	.46
11	.55	.23
12	.19	.13
13	0.38	0.38
14	.35	.23
15	.53	.15
16	.79	.05
17	0.38	0.38
18	.39	.28
19	.45	.39
20	.20	.59
21	0.80	0.43
22	.40	.19
23	.45	.26
24	.40	.13
25	0.08	0.61
26	.32	.47
27	.51	.32
28	.34	.32
29	0.40	0.14
30	.47	.22
31	.46	.26
32	.16	.50
Average	0.35	0.28

TABLE IV.—ANALYTICAL AND EXPERIMENTAL PERFORMANCES OF TWT 204 AND 1.7-CENTIMETER-DIAMETER, FOUR-STAGE, DEPRESSED COLLECTOR, WITH TWT OPERATING AT SATURATION AND ANALYTICALLY DETERMINED COLLECTOR VOLTAGES

[Computed trajectories shown in fig. 5. Voltages, currents, and powers given as percentages of V_0, I_0, and V_0I_0, respectively.]

(a) MDC performance

Collecting element	Voltage	Analytical			Experimental		
		Current	Recovered power	Kinetic power dissipated	Current	Recovered power	Kinetic power dissipated
TWT body (interception)	0	4.1	0	4.1	1.9	0	1.9
TWT body (backstreaming)	0	4.2	0	3.2	1.8	0	(a)
Electrode:							
1	50.0	3.1	1.6	.2	5.1	2.6	(a)
2	61.4	43.0	26.4	4.1	60.0	36.8	(a)
3	82.8	42.5	35.2	5.4	29.5	24.4	(a)
4	100.0	3.0	3.0	.7	1.7	1.7	(a)
Collector efficiency, percent		82.9			80.2		
Overall efficiency, percent		39.9			35.4		

(b) Final power distribution

Components of power	Analytical	Experimental
RF output power	13.5	12.3
Total RF power losses (including circuit and sever losses)	2.7	4.1
Beam interception losses	4.1 } 20.4	1.9 } 22.0
Backstreaming to TWT body	3.2	(a)
MDC dissipation	10.4	(a)
Recovered power	66.1	65.6

[a]Not measured.

TABLE V.—ANALYTICAL AND EXPERIMENTAL PERFORMANCES OF TWT 204 AND 1.7-CENTIMETER-DIAMETER, FOUR-STAGE, DEPRESSED COLLECTOR, WITH TWT OPERATING AT SATURATION AND INTERMEDIATE COLLECTOR VOLTAGES

[Computed trajectories shown in fig. 6. Voltages, currents, and powers given as percentages of V_0, I_0, and V_0I_0, respectively.]

(a) MDC performance

Collecting element	Voltage	Analytical			Experimental		
		Current	Recovered power	Kinetic power dissipated	Current	Recovered power	Kinetic power dissipated
TWT body (interception)	0	4.1	0	4.1	1.9	0	1.9
TWT body (backstreaming)	0	4.1	0	2.4	1.4	0	(a)
Electrode:							
1	53.7	15.6	8.4	1.6	6.2	3.3	(a)
2	66.2	27.6	18.3	2.4	58.2	38.5	(a)
3	82.3	45.5	37.5	5.7	30.7	25.3	(a)
4	100.0	3.0	3.0	.7	1.7	1.7	(a)
Collector efficiency, percent		84.1			84.3		
Overall efficiency, percent		41.0			39.4		

(b) Final power distribution

Components of power	Analytical	Experimental
RF output power	13.5	12.3
Total RF power losses (including circuit and sever losses)	2.7	4.1
Beam interception losses	4.1 } 19.5	1.9 } 19.0
Backstreaming to TWT body	2.4	(a)
MDC dissipation	10.3	(a)
Recovered power	67.1	68.8

[a]Not measured.

TABLE VI.—ANALYTICAL AND EXPERIMENTAL PERFORMANCES OF TWT 204 AND 1.7-CENTIMETER-DIAMETER, FOUR-STAGE, DEPRESSED COLLECTOR, WITH TWT OPERATING AT SATURATION AND EXPERIMENTALLY OPTIMIZED COLLECTOR VOLTAGES

[Computed trajectories shown in fig. 7. Voltages, currents, and powers given as percentages of V_0, I_0, and V_0I_0, respectively.]

(a) MDC performance

Collecting element	Voltage	Analytical			Experimental		
		Current	Recovered power	Kinetic power dissipated	Current	Recovered power	Kinetic power dissipated
TWT body (interception)	0	4.1	0	4.1	1.9	0	1.9
TWT body (backstreaming)	0	3.1	0	1.7	1.1	0	(a)
Electrode:							
1	57.3	21.0	12.1	1.6	9.5	5.4	(a)
2	68.9	23.2	16.0	1.6	53.7	37.0	(a)
3	81.5	45.5	37.1	6.0	32.2	26.3	(a)
4	100.0	3.0	3.0	.7	1.6	1.6	(a)
Collector efficiency, percent		85.4			86.2		
Overall efficiency, percent		42.3			41.6		

(b) Final power distribution

Components of power	Analytical	Experimental
RF output power	13.5	12.3
Total RF power losses (including circuit and sever losses)	2.7	4.1
Beam interception losses	4.1	1.9
Backstreaming to TWT body	1.7	(a)
MDC dissipation	10.0	(a)
	18.4	17.5
Recovered power	68.1	70.4

[a]Not measured.

TABLE VII.—ANALYTICAL AND EXPERIMENTAL PERFORMANCES OF TWT 204 AND 1.7-CENTIMETER-DIAMETER, FOUR-STAGE, DEPRESSED COLLECTOR, WITH TWT OPERATING AT SATURATION AND COLLECTOR VOLTAGES SELECTED EXPERIMENTALLY FOR OPERATION AT 8 TO 15.5 GHz

[Computed trajectories shown in fig. 8. Voltages, currents, and powers given as percentages of V_0, I_0, and V_0I_0, respectively.]

(a) MDC performance

Collecting element	Voltage	Analytical, at 13 GHz		Experimental, at 13 GHz		Experimental, at 15 GHz	
		Current	Recovered power	Current	Recovered power	Current power	Recovered
TWT body (interception)	0	4.1	0	1.9	0	1.9	0
TWT body (backstreaming)	0	1.0	0	1.0	0	1.4	0
Electrode:							
1	50.1	18.7	9.4	7.0	3.5	9.1	4.6
2	66.7	25.0	16.7	45.2	30.2	49.3	32.9
3	77.2	49.8	38.5	44.2	34.1	37.8	29.2
4	100.0	1.3	1.3	.9	.9	.6	.6
Collector efficiency, percent		82.4		84.1		84.5	
Overall efficiency, percent		39.4		39.4		41.2	

(b) Final power distribution

Components of power	Analytical, at 13 GHz	Experimental, at 13 GHz	Experimental, at 15 GHz
RF output power	13.5	12.3	13.5
Total RF power losses (including circuit and sever losses)	2.7	4.1	5.0
Beam interception losses	4.1 } 20.8	1.9 } 19.1	1.9 } 19.0
Backstreaming to TWT body	.7	(a)	(a)
MDC dissipation	13.3	(a)	(a)
Recovered power	65.8	68.7	67.3

[a]Not measured.

TABLE VIII.—SUMMARY OF ANALYTICAL VERSUS EXPERIMENTAL RESULTS FOR TWT 204 AND MDC, WITH TWT OPERATING AT SATURATION AT 13 GHz

(a) Four-stage collector

MDC operating condition	Overall efficiency, percent		Collector efficiency, percent	
	Analytical	Experimental	Analytical	Experimental
Design voltages	39.9	35.7	82.9	80.2
Intermediate voltages	41.0	39.4	84.1	84.3
Experimentally optimized voltages	42.3	41.6	85.4	86.2
Set voltages for 8 to 15.5 GHz data	39.4	39.4	82.4	84.1

(b) Three-stage collector

Design voltages	36.1	31.0	78.4	74.1
Intermediate voltages	36.2	33.4	78.6	77.4
Experimentally optimized voltages	35.7	36.3	78.0	81.0

TABLE IX.—COMPUTED TWT AND MDC EFFICIENCIES WITH AND WITHOUT SECONDARY ELECTRON EMISSION LOSSES, WITH TWT OPERATING AT SATURATION AT 13 GHz

(a) Overall TWT efficiency

MDC operating condition	Efficiency, percent	
	Without secondary electron emission losses	With secondary electron emission losses
Design voltages	45.6	39.9
Intermediate voltages	43.0	41.0
Experimentally optimized voltages	43.4	42.3
Set voltages for 8- to 15.5-GHz data	40.1	39.4

(b) Collector efficiency

Design voltages	88.2	82.9
Intermediate voltages	86.0	84.1
Experimentally optimized voltages	86.4	85.4
Set voltages for 8- to 15.5-GHz data	83.2	82.4

TABLE X.—ANALYTICAL PERFORMANCES OF VARIAN VTM-6294 TWT AND THREE-STAGE AND SIMULATED THREE-STAGE COLLECTORS, WITH TWT OPERATING AT SATURATION AT 13 GHz

[Computed trajectories shown in figs. 10 and 11. Voltages and currents given as percentages of V_0 and I_0, respectively.]

Collecting element	Voltage	Three-stage design current	Three-stage simulation design current
TWT body (interception)	0	4.1	4.1
TWT body (backstreaming)	0	5.5	4.3
Electrode:			
1	53.8	45.5	47.3
2	82.8	42.1	41.2
3	100	2.7	3.0
Collector efficiency, percent		77.8	78.4
Overall efficiency, percent		35.6	36.1

TABLE XI.—ANALYTICAL AND EXPERIMENTAL PERFORMANCES OF TWT 204 AND 1.7-CENTIMETER-DIAMETER, THREE-STAGE, DEPRESSED COLLECTOR, WITH TWT OPERATING AT SATURATION AND ANALYTICALLY DETERMINED COLLECTOR VOLTAGES

[Computed trajectories shown in fig. 11. Voltages, currents, and powers given as percentages of V_0, I_0, and V_0I_0, respectively.]

(a) MDC performance

Collecting element	Voltage	Analytical			Experimental		
		Current	Recovered power	Kinetic power dissipated	Current	Recovered power	Kinetic power dissipated
TWT body (interception)	0	4.1	0	4.1	1.9	0	1.9
TWT body (backstreaming)	0	4.3	0	3.6	2.8	0	(a)
Electrode:							
1a	53.8	3.1	1.7	0	5.9	3.2	(a)
1b	53.8	44.2	23.7	7.5	58.7	31.5	(a)
2	82.8	41.2	34.1	5.4	29.2	24.2	(a)
3	100.0	3.0	3.0	.7	1.6	1.6	(a)
Collector efficiency, percent		78.4			74.1		
Overall efficiency, percent		36.1			31.0		

(b) Final power distribution

Components of power	Analytical	Experimental
RF output power	13.5	12.2
Total RF power losses (including circuit and sever losses)	2.7	4.1
Beam interception losses	4.1 } 24.0	1.9 } 27.1
Backstreaming to TWT body	3.6	(a)
MDC dissipation	13.6	(a)
Recovered power	62.6	60.6

[a]Not measured.

TABLE XII.—ANALYTICAL AND EXPERIMENTAL PERFORMANCES OF TWT 204 AND 1.7-CENTIMETER-DIAMETER, THREE-STAGE, DEPRESSED COLLECTOR, WITH TWT OPERATING AT SATURATION AND INTERMEDIATE COLLECTOR VOLTAGES

[Computed trajectories shown in fig. 12. Voltages, currents, and powers given as percentages of V_0, I_0, and V_0I_0, respectively.]

(a) MDC performance

Collecting element	Voltage	Analytical			Experimental		
		Current	Recovered power	Kinetic power dissipated	Current	Recovered power	Kinetic power dissipated
TWT body (interception)	0	4.1	0	4.1	1.9	0	1.9
TWT body (backstreaming)	0	3.1	0	1.7	2.5	0	(a)
Electrode:							
1a	55.5	0	0	0	3.7	2.0	(a)
1b	55.5	44.0	24.4	6.7	47.7	26.5	(a)
2	78.1	47.3	36.9	8.3	43.3	33.8	(a)
3	100.0	1.4	1.4	.3	.9	.9	(a)
Collector efficiency, percent		78.6			77.4		
Overall efficiency, percent		36.2			33.4		

(b) Final power distribution

Components of power	Analytical	Experimental
RF output power	13.5	12.3
Total RF power losses (including circuit and sever losses)	2.7	4.1
Beam interception losses	4.1 } 23.8	1.9 } 24.4
Backstreaming to TWT body	1.7	(a)
MDC dissipation	15.3	(a)
Recovered power	62.8	63.3

[a]Not measured.

TABLE XIII.—ANALYTICAL AND EXPERIMENTAL PERFORMANCES OF TWT 204 AND 1.7-CENTIMETER-DIAMETER, THREE-STAGE, DEPRESSED COLLECTOR, WITH TWT OPERATING AT SATURATION AND EXPERIMENTALLY OPTIMIZED COLLECTOR VOLTAGES

[Computed trajectories shown in fig. 13. Voltages, currents, and powers given as percentages of V_0, I_0, and V_0I_0, respectively.]

(a) MDC performance

Collecting element	Voltage	Analytical			Experimental		
		Current	Recovered power	Kinetic power dissipated	Current	Recovered power	Kinetic power dissipated
TWT body (interception)	0	4.1	0	4.1	1.9	0	1.9
TWT body (backstreaming)	0	3.1	0	1.7	.6	0	(a)
Electrode:							
1a	57.3	1.6	1.0	.3	3.5	2.0	(a)
1b	57.3	35.3	20.2	4.0	29.5	16.9	(a)
2	73.0	54.4	39.7	11.2	64.4	47.0	(a)
3	100.0	1.4	1.4	.3	.3	.3	(a)
Collector efficiency, percent		78.0			81.0		
Overall efficiency, percent		35.7			36.3		

(b) Final power distribution

Components of power	Analytical	Experimental
RF output power	13.5	12.3
Total RF power losses (including circuit and sever losses)	2.7	4.1
Beam interception losses	4.1 } 24.3	1.9 } 21.7
Backstreaming to TWT body	1.7	(a)
MDC dissipation	15.8	(a)
Recovered power	62.2	66.2

[a]Not measured.

TABLE XIV.—COMPUTED TWT AND THREE-STAGE COLLECTOR EFFICIENCIES WITH AND WITHOUT SECONDARY ELECTRON EMISSION LOSSES, WITH TWT OPERATING AT SATURATION AT 13 GHz

(a) Overall TWT efficiency

MDC operating condition	Efficiency, percent	
	Without secondary electron emission losses	With secondary electron emission losses
Design case voltages	41.2	36.1
Intermediate voltages	37.0	36.2
Experimentally optimized voltages	36.7	35.7

(b) Collector efficiency

Design case voltages	84.3	78.4
Intermediate voltages	79.6	78.6
Experimentally optimized voltages	79.3	78.0

TABLE XV.—AVERAGE PERFORMANCE OF TWT 204 AND MDC ACROSS OPERATING BAND OF 8 TO 15.5 GHz AT SATURATION

RF efficiency, percent	12.4
Overall efficiency, percent	38.7
Collector efficiency, percent	83.2

1. Report No.	2. Government Accession No.	3. Recipient's Catalog No.
NASA TP-2524		

4. Title and Subtitle	5. Report Date
Verification of Computer-Aided Designs of Traveling-Wave Tubes Utilizing Novel Dynamic Refocusers and Graphite Electrodes for the Multistage Depressed Collector	October 1985
	6. Performing Organization Code: 506-58-22
7. Author(s): Peter Ramins, Henry G. Kosmahl, Dale A. Force, Raymond W. Palmer, and James A. Dayton, Jr.	8. Performing Organization Report No.: E-2566
	10. Work Unit No.
9. Performing Organization Name and Address: National Aeronautics and Space Administration, Lewis Research Center, Cleveland, Ohio 44135	11. Contract or Grant No.
	13. Type of Report and Period Covered: Tecnnical Paper
12. Sponsoring Agency Name and Address: National Aeronautics and Space Administration, Washington, D.C. 20546	14. Sponsoring Agency Code

15. Supplementary Notes

16. Abstract

A computational procedure for the design of TWT-refocuser-MDC systems was used to design a short "dynamic refocusing" system and highly efficient four-stage depressed collector for a 200-W, 8- to 18-GHz, TWT. The computations were carried out with advanced, multidimensional computer programs which model the electron beam as a series of disks of charge and follow their trajectories from the RF input of the TWT, through the slow-wave structure and refocusing section, to their points of impact in the depressed collector. Secondary emission losses in the MDC were treated semi-quantitatively by injecting a representative beam of secondary electrons into the MDC analysis at the point of impact of each primary beam. A comparison of computed and measured TWT and MDC performance showed very good agreement. The electrodes of the MDC were fabricated from a particular form of isotropic graphite that was selected for its low secondary electron yield, ease of machinability, and vacuum properties. This MDC was tested (at CW) for more than 1000 hr with negligible degradation in TWT and MDC performances.

17. Key Words (Suggested by Author(s))	18. Distribution Statement
Traveling-wave tube Multistage depressed collector	Unclassified - unlimited STAR Category 33

19. Security Classif. (of this report)	20. Security Classif. (of this page)	21. No. of pages	22. Price*
Unclassified	Unclassified	25	A02

*For sale by the National Technical Information Service, Springfield, Virginia 22161

NASA-Langley, 1985

National Aeronautics and
Space Administration
Code NIT-3

Washington, D.C.
20546-0001